

CFD MODELING OF ALUMINA SLURRY HEAT EXCHANGER HEADERS: (ii) PARAMETRIC STUDIES

Matthew BRENNAN¹, Klaus BREMHORST²

¹The Julius Kruttschnitt Mineral Research Centre, The University of Queensland, 40 Isles Rd, Indooroopilly, Queensland, 4068, AUSTRALIA

²School of Engineering, The University of Queensland, Brisbane, Queensland, 4072, AUSTRALIA

ABSTRACT

CFD simulations have been conducted of the inlet header of an industrial scale parallel pass alumina slurry heat exchanger. The CFD modelling used an accurate geometric model of the header where the tube plate and the first 600 mm of each tube in the pass are included in the CFD grid. The simulations looked at a number of inlet configurations including side and axial entry. The results suggest that the flow at the tube sheet in a standard side entry inlet header is asymmetric with large angles of attack on parts of the tube sheet which leads to flow separation in the entrances to the tubes, a phenomenon which correlates with erosion and corrosion in the tube inlets. Axial entry to the header is a more satisfactory configuration but flow characteristics are influenced by the inlet pipe.

NOMENCLATURE

C_m	inertial porous resistance coefficient
p	pressure, kPa
r	radial position in pipe, m
u	slurry velocity, m.s ⁻¹
α	velocity angle relative to header axis (degrees)
ρ	density, kg.m ⁻³

SI units have been used generally in this paper, however the derived unit mm has been used.

INTRODUCTION

Shell and tube heat exchangers are used for heat recovery in the Bayer Alumina Process. The heat exchangers are typically standard TEMA (Tubular Exchanger Manufacturers Association, Inc.) side entry designs and are constructed of mild steel. Modern practice is to heat the feed slurry to the alumina digesters with steam obtained from flash cooling of the product stream from the digester. The feed slurry is aqueous caustic soda with a suspended bauxite concentration of typically 10-15% to give an overall slurry density of around 1400 kg.m⁻³.

As might be expected, operation of heaters with such feed materials imposes major maintenance costs. A number of characteristic forms of heater damage have been identified, with tube plate worming, tube blockage and

tube inlet failure being the main causes of heater failure. (Lai and Bremhorst 1979, Bremhorst and Flint 1991) However these problems occur primarily on the 1st pass inlet header with the subsequent passes operating satisfactorily.

A major underlying mechanism has been identified as erosion/corrosion where impingement of solid particles on the heater surfaces prevents the build up of a passivating film that would otherwise protect the metal surfaces. Erosion/corrosion is heavily influenced by the hydrodynamics. In particular tube damage primarily occurs in the tube inlets in regions of the tube sheet where there is a high velocity angle of the slurry which leads to flow separation in the tube inlets.

It is known that the standard TEMA side entry inlet header has undesirable hydrodynamics with the side entry flow generating a vortex along the axis of the heater (Bremhorst and Brennan, 2009) and the recoil of the flow from the pass separation baffle generates very large angles of attack at the tube sheet (defined as α in this paper in equation (3) in the next section). These two effects combine to cause flow separation in the tube entrances, an effect which is correlated with tube inlet failure. As discussed by Elvery and Bremhorst (1996), flow separation starts to occur in the tube entrances when α exceeds 30° and a more optimal header design would therefore reduce α to less than 30° over preferably all of the tube sheet.

In this paper the methodology for modelling the inlet and pass headers of industrial heat exchangers using Computational Fluid Dynamics (CFD) described in Bremhorst and Brennan (2009) has been applied in a series of parametric studies. The effects of changes to the geometry of the inlet header of an industrial alumina slurry heater on critical hydrodynamic characteristics have been investigated. The aim of the work has been to establish more optimal inlet header designs. Minimising α has been chosen as the main criteria of hydrodynamic quality.

MODEL DESCRIPTION

Grid Generation

The CFD simulations used an accurate geometric model of the heater inlet header, which was set up in Gambit (within FLUENT). All geometries were based on a 1772 mm ID heater with 274 33mm ID tubes on a 47.625mm triangular pitch. A rendering of the side entry geometry

that was used as the base geometry for the study is shown in Figure 1. The CFD used the “with tubes” approach, outlined in Bremhorst and Brennan (2009) where the first 600 mm of each tube in the pass was included in the simulation as a region of turbulent flow and an additional 300 mm of tube length was included as a separate porous zone. This required a 900 mm length of each tube to be included in the grid. (See the next section for more details). A 600 mm length of the slurry inlet pipe to the header was also included in the grid.

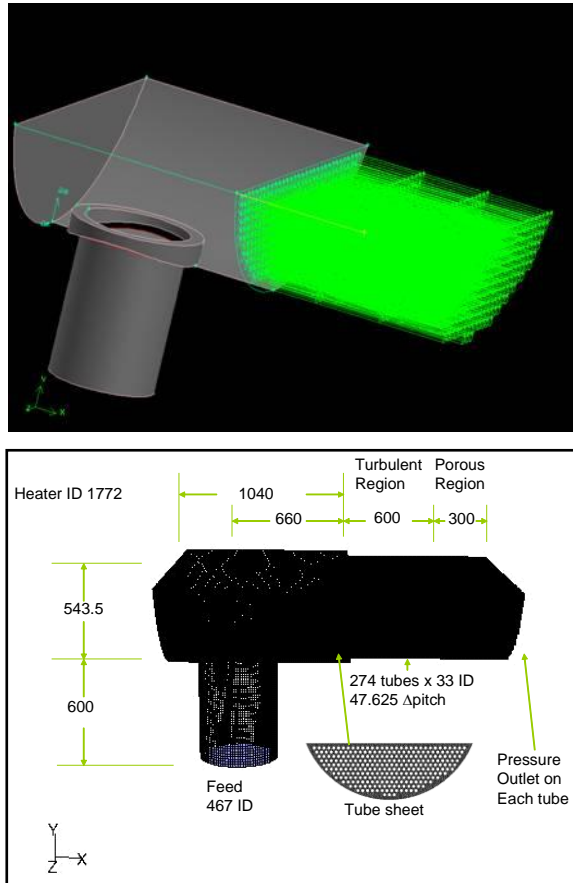


Figure 1. Rendering of base side entry geometry in Gambit.

The flow domain was meshed with a 20 mm unstructured tetrahedral mesh in the header space. The face mesh on the tube plate and each face on the tube inlet were meshed with a 7.5 mm tri paved mesh. The feed pipe was meshed with a 20 mm Cooper mesh using the 20mm tri face mesh at the boundary between the pipe and the header as the projecting mesh. Each tube was meshed with the Cooper mesh using the inlet face as the projecting face mesh. The first 600 mm of each tube used a graded axial mesh from 7.5 to 120 mm. The last 300 mm of each tube needed to be a separate fluid zone and used a 120 mm axial mesh. The grids typically had 8.0×10^5 nodes.

The feed pipe inlet used a velocity inlet boundary condition, all tube outlets used a pressure outlet boundary condition and all other boundaries were walls, including the tube plate.

CFD modeling

The CFD simulations were solved using Fluent 6.2.15 and later Fluent 6.3.26. The cases were set up using a single phase fluid with a density of 1400 kg.m^{-3} and a viscosity

of $0.005 \text{ kg.m}^{-1}.\text{s}^{-1}$, which are equivalent to the density and viscosity of Bayer liquor with 10% alumina by volume. The SST $k-\omega$ model (Menter 1992) was used. A comparison between the SST $k-\omega$ model (Menter 1992) and LES results on similar geometries is discussed in the accompanying paper (Bremhorst and Brennan 2009). The segregated solver was used with PRESTO for pressure and 3RD order MUSCL for all other transport equations and SIMPLE for the pressure velocity coupling.

A velocity profile was applied to the feed boundary condition using the relationship for fully developed turbulent flow from Bird et al (1960):

$$\frac{u(r)}{u_{\max}} = \left(1 - \frac{r}{R_p}\right)^{1/7} \quad (1)$$

As discussed in Bremhorst and Brennan (2009), the correct pressure drop for a 8m tube bundle was obtained by making the last 300 mm of each tube a separate fluid zone and adjusting the porosity only in this zone. The Fluent porous model has two options for introducing additional resistance to flow, of which the inertial option was used:

$$\nabla p = C_{in} \frac{1}{2} \rho u_x |\mathbf{u}| \quad (2)$$

An isotropic resistance was used and C_{in} was adjusted so to give a header pressure of 45 kPa at the tube plate. The first 600 mm of each tube was treated as turbulent flow, so the porous zone was 18 tube diameters downstream of the tube entrances. The tube Reynolds number at rated slurry flow is around 19000, which is turbulent. Mulley (2004) recommends that 30 tube diameters are needed for a fully developed turbulent flow profile to be established in pipes. Figure 2 shows contours of velocity in a typical tube at 300 mm and 500 mm from the tube plate. These plots indicate that the velocity profiles are approaching constant values before the porous zone is approached. However Figure 2 also indicates that the 7.5mm tri grid normal to the direction of flow in the tubes is coarse and as noted in the next paragraph grid refinement has been used to better resolve flow in the tube entrances.

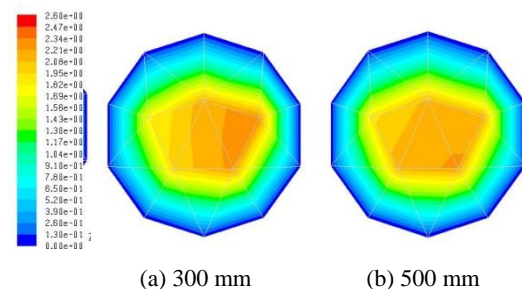


Figure 2. Contours of velocity (m.s^{-1}) in tube at 300 mm and 500 mm from tube plate. Original unrefined 7.5 mm tri grid is superimposed.

The cases were initialized and solved using the steady segregated solver for approximately 4000 iterations, after which the unsteady solver was enabled and the case was integrated over time. Solution using the unsteady solver from initialization was found to converge on identical results but took longer. The criterion used for convergence was not just minimum residuals (which were set at 10^{-5}), but that the flow field reached a steady flow, as evidenced

by unchanging angles of attack at the tube sheet. Steady flow was achieved after 50s of simulation time but cases were integrated to 100s. After convergence the grids were refined in the vicinity of the tube sheet (from -0.15 to +0.3m) using the standard Fluent algorithm to better resolve the flow separation in the tubes inlets and the refined grid cases were solved to convergence and saved as separate cases.

Results for standard side entry header at rated flow

The velocity angle of the slurry, 10 mm upstream from the tube sheet, is used in this study as the criterion of the quality of the flow. This is defined as angle of the velocity vector relative to the axis of the heater, which in all geometries is the x axis and has been calculated in a custom field function with the formula:

$$\alpha = \frac{180}{\pi} \sin^{-1} \left(\frac{\sqrt{u_y^2 + u_z^2}}{|u|} \right) \quad (3)$$

Figure 3 shows the contours of velocity angle across the tube sheet at the rated heater feed flow rate of 638 kg.s⁻¹. Figure 4 shows the contours of axial velocity in the y plane at an elevation of 0.42m, which intersects the third row of tubes is near the position shown by the arrow on Figure 3. As can be seen the angles of attack across the entire tube sheet are large and there is flow separation occurring within the tubes near the arrow as evidenced by the axial velocity becoming negative on the RHS of each the 4th through 7th tubes on Figure 4. (The range of the plot on Figure 4, Figure 7 & Figure 8 has been limited to -0.5 to 1.0 m.s⁻¹ to highlight flow separation. The actual maximum tube velocities is much higher, typically being from 2.1 to 4 m.s⁻¹)

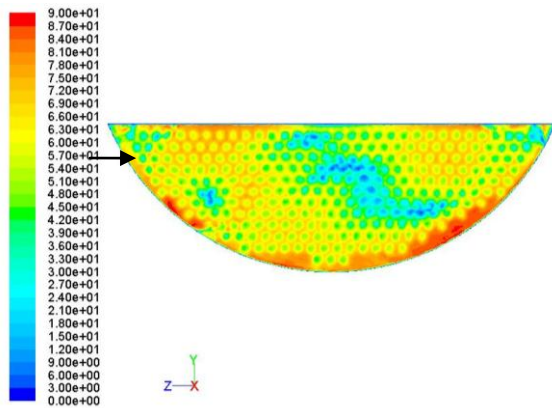


Figure 3. Contours of velocity angle 10 mm upstream of tube sheet at rated feed slurry flow rate of 638 kg.s⁻¹. Arrow indicates y elevation of 0.42m.

Results for standard side entry header at different slurry flow rates

Simulations at slurry feed flow rates of 70% and 130% of rated flow were generated. The contours of velocity angle show that the velocity angles become worse when the slurry flow rate is reduced (Figure 5, 70% rated flow) and improve somewhat, but are still poor, when the slurry flow rate is increased (Figure 6, 130% rated flow). The velocities at y=0.42m (Figure 7, 70% rated flow and Figure 8, 130% rated flow)) show that flow separation continues to occur over this range of feed slurry flow rates. However flow separation seems less pronounced at higher slurry flow rates.

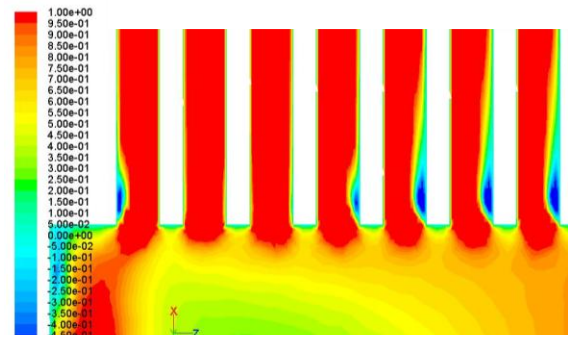


Figure 4. Contours of axial velocity for 1st to 7th tubes from LHS of header at y = 0.42m at rated slurry feed flow rate. Contour plot range has been limited to -0.5 to 1.0 m.s⁻¹ to emphasize the regions of flow separation.

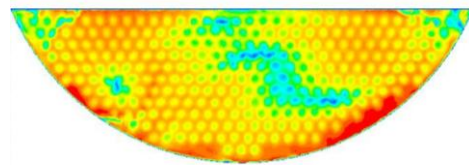


Figure 5. Contours of velocity angle 10 mm upstream of tube sheet at 70% rated slurry feed flow rate. (Colour range is the same as Figure 3)

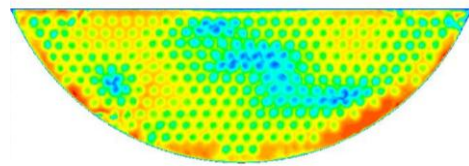


Figure 6. Contours of velocity angle 10 mm upstream of tube sheet at 130% rated slurry feed flow rate. (Colour range is the same as Figure 3)

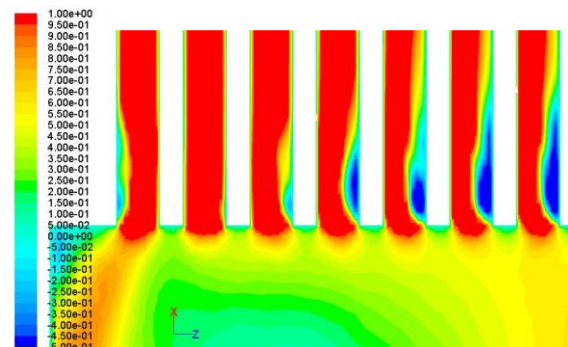


Figure 7. Contours of axial for 1st 7 tubes from LHS of header at y = 0.42m at 70% rated slurry feed flow rate. Contour plot range has been limited to -0.5 to 1.0 m.s⁻¹ to emphasize the regions of flow separation.

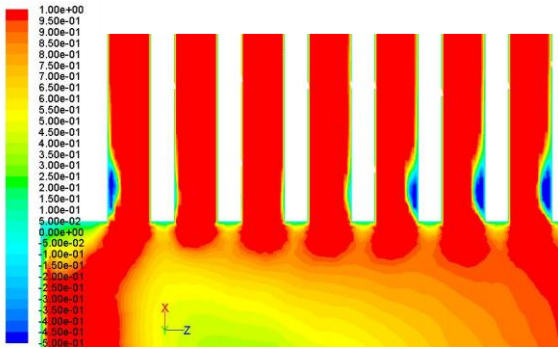


Figure 8. Contours of axial velocity for 1st 7 tubes from LHS of header at $y = 0.42\text{m}$ at 130% rated slurry feed flow rate. Contour plot range has been limited to -0.5 to $1.0\text{ m}\cdot\text{s}^{-1}$ to emphasise the regions of flow separation.

Results for axial entry header at rated slurry flow rate

The major problem with the side entry header (as discussed in Bremhorst and Brennan, 2009) is that the flow exits from the inlet pipe and hits the opposing pass baffle. The slurry then spreads and recoils and flows down the shell as it flows towards the tube sheet. There are a number of options for improving the hydrodynamics, including inserts, making the header longer (so giving the flow a chance to recover) and changing to an alternative flow configuration such as axial entry. As noted below reducing the velocity angles is hampered when there are bends on the inlet pipe.

A series of grids were generated for the same header and pipe configuration as shown in Figure 1 but with the feed pipe oriented axially. A 1000mm length of 467 mm ID pipe was simulated with a velocity inlet boundary condition with the turbulent velocity profile given by equation (1).

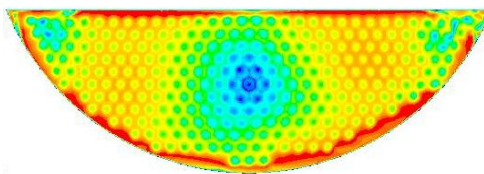


Figure 9. Contours of velocity angle, 10 mm upstream from tube sheet for axial entry header at rated slurry flow rate (Colour range is the same as Figure 3)

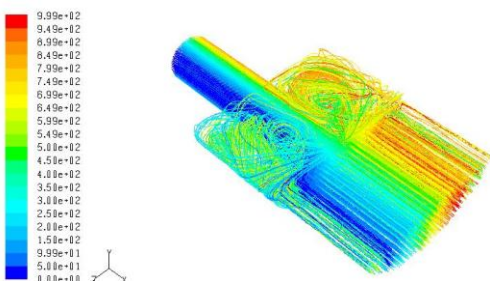


Figure 10. Velocity pathlines for axial entry header at rated slurry flow rate.

Figure 9 shows the contours of velocity angle and they indicate a different flow pattern with a very low velocity angle at the tube plate centre due to the jet from the inlet

pipe but the angles of attack are still very poor outside this central region. Velocity pathlines (Figure 10) show that the 1040 mm length of header is insufficient for the jet to spread.

The angles of attack could be improved in a number of ways. One is to make the header longer, but this is problematical because the overall length, weight and therefore the cost of the heat exchanger are all increased. Further a longer header creates a large space where solids can accumulate. The other option is to investigate shaping the entry to the header.

Results for axial entry header with flared inlet nozzle at rated slurry flow rate

Three grids were developed and which used the same dimensions as the axial inlet header but where the inlet pipe was flared into an elliptical diffuser. The length of the flared section was kept at 500 mm and 500 mm of inlet pipe was included in the simulations. A rendering of the 467x667 mm flare is shown in Figure 11.

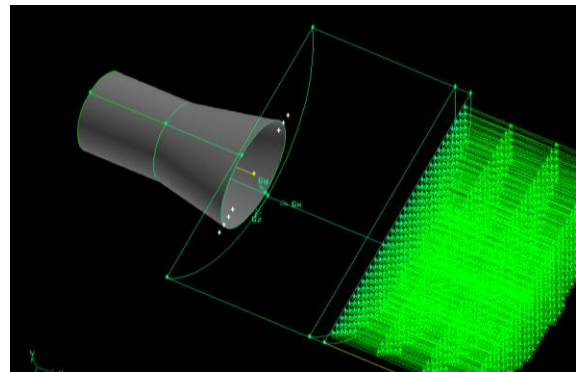


Figure 11. Rendering of 467x667 mm flared inlet

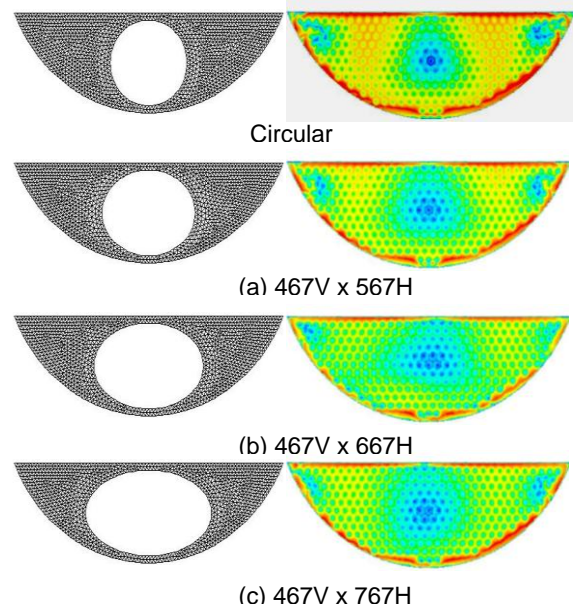


Figure 12. Contours of velocity angle, 10 mm upstream from tube sheet, axial entry header, flaring of inlet nozzle, rated slurry flow rate. V and H are the minor and major diameters in mm of ellipse at header inlet. (Colour range is the same as Figure 3)

Figure 12 shows the contours of the velocity angle for these three geometries with the circular geometry for comparison. (The contours for the 467x667 insert are shown in larger scale on Figure 14a.) The dimensions of each diffuser at the end plate are also shown on Figure 12. Whilst introducing an elliptical flare into the inlet pipe is a design and structural complication, the flare gives the flow a chance to “pre-spread” and as can be seen, flaring the inlet pipe considerably reduces the velocity angle, though there are regions where the velocity angle at the tube sheet are still around 50° (yellow).

Results for axial entry header with flared inlet nozzle extended into the header at rated slurry flow rate

A grid was developed using the 467x667 mm flare where an additional section was inserted into the header space such that the inlet path was shaped from the ellipse of the diffuser at the end plate to the chord shape of the header 100 mm from the tube plate. A rendering of this geometry is shown in Figure 13. The contours of the velocity angle with and without the extension are shown in Figure 14. What is interesting is that the extension shown on Figure 13, perhaps counter-intuitively, makes the velocity angle at the tube sheet worse. A number of other header inserts of this type have been investigated and all consistently worsen the angles of attack. A general conclusion from this is that any flow inserts should be a nozzle that shapes the flow into the header, but once the flow is in the header it should be allowed to spread as a free jet.

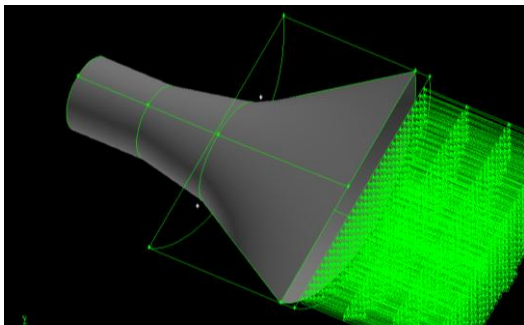
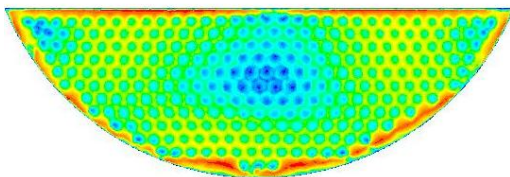
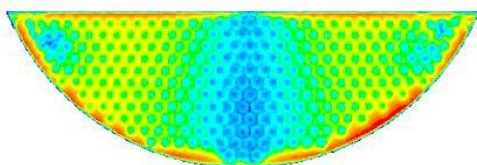


Figure 13. Rendering of 467x667 mm flared inlet with header insert.



(a) 467V x 667H flared inlet to end plate (Figure 11)



(b) 467V x 667H flared inlet with header insert (Figure 13)

Figure 14. Contours of velocity angle, 467V x 667H mm flared inlet pipe, (a) without and (b) with internal header insert. (Colour range is the same as Figure 3)

Results for axial headers 2D and 4D bends on inlet pipe

Industrial heat exchangers are connected with process piping and plant layout practice dictates that piping should be kept as short as possible. Inevitably this means that the inlet piping will have a 90 degree bend only a short distance from the header. Lai and Bremhorst (1979) showed that varying the inlet pipe angle relative to the axis had an effect in measured velocities at the tube plate in studies of an experimental heat exchanger, which was of a side entry design. Disturbance of the flow due to the inlet piping is likely to be more of a problem with any axial entry arrangement when compared to the side entry design because the side entry disturbs the flow in a way which would tend to destroy any flow history effects from further upstream, in a way that would not occur in an axial header.

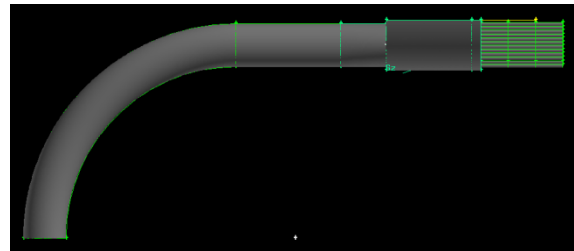
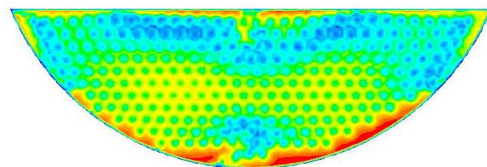
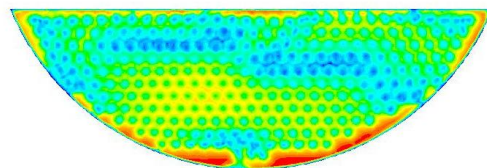


Figure 15. Axial entry header with 1870 mm R bend added 1650 mm from end plate

Two grids were generated with a 90° bend added onto the inlet pipe, oriented in the $-y$ direction. Figure 15, shows the arrangement for the grid with a 1870 mm ($4D_{\text{pipe}}$) radius bend and the second grid had a 934mm ($2D_{\text{pipe}}$) radius bend. Both grids used a 467V x 667H flared inlet at the header.



(a) 934 mm radius bend



(b) 1870 mm radius bend

Figure 16. Contours of velocity angle at rated flow, 10 mm from tube plate, axial entry header 467V x 667H mm flared inlet nozzle, 90° bend attached to inlet pipe (Colour range is the same as Figure 3)

The contours of velocity angle for both the 934 mm radius and 1870 mm radius bends shown in Figure 16 indicate that both bends have a fairly significant effect on flow in the header, with the region where the angles of attack shifted to the upper part of the header compared to the simulation for the same geometry without the inlet pipe. This is essentially because the hydraulic force of the slurry introduces an asymmetry into the flow as it passes around

the bend, shown clearly in contours of axial velocity in the straight pipe section just after the bend in Figure 17.

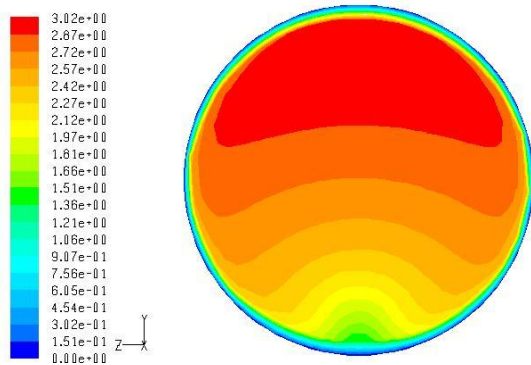


Figure 17. Contours of axial velocity (m.s^{-1}) at rated flow in inlet pipe 810 mm from header end plate, for axial entry header, 467V c 667H mm flared inlet nozzle and 1870 mm radius bend

The inlet pipe configuration depends on particular plant designs and therefore an exact conclusion really cannot be drawn. Making the straight section between the bend and the flare longer would help but it is likely that the straight section in the configurations modeled here is as long as practical.

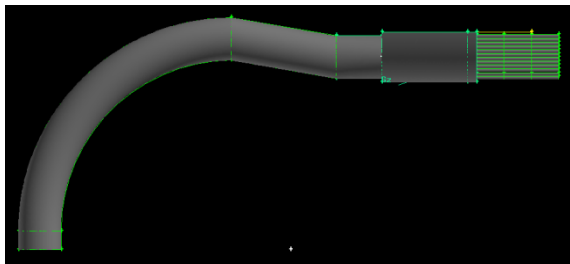


Figure 18. Axial entry header with 1870 mm radius bend added 1650 mm from end plate but displaced 200 mm inwards toward heater centre.

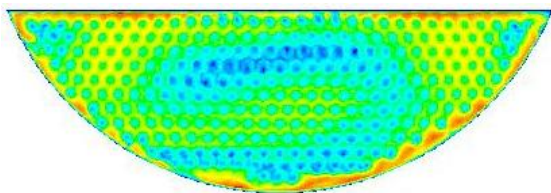


Figure 19. Contours of velocity angle at rated flow, 10 mm from tube plate, axial entry header, 1870 mm radius bend added 1650 mm from end plate but displaced 200 mm inwards toward heater centre. (Colour range is the same as Figure 3)

A grid (rendering shown on Figure 18) was generated where the inlet pipe bend was displaced inwards to the heater centre by 200 mm and the cylindrical section was angled outwards. The contours of velocity angle as shown on Figure 19 indicate that the jet has been displaced down, but it is debatable whether the overall angles of attack have been improved. Table 1 shows the mean and standard deviation of the velocity angle for the base side entry (Figure 3), axial with flare (Figure 12b) and axial with flare and displaced bend (Figure 19). This table indicates that axial with a flare considerably improves the flow

hydrodynamics, although there are still regions at the tube sheet where the velocity angle is greater than 30° .

Header	α_{av}	SD on α
Side	55.7	16
Axial + 467x667	36	20
Axial + 467x667 b 200	38	19

Table 1 Mean velocity angle and standard deviation, 10 mm from tube sheet at rated flow for base side entry header, Axial + 467x667 flare and Axial + 467x667 flare and 1870mm radius bend displaced 200mm

CONCLUSION

A series of CFD simulations in Fluent have been conducted of the inlet header of a 1770mm ID parallel pass heat exchanger with a full simulation of the tube plate and all 274 tubes in the pass. This heater is typical of the heat exchangers used for primary slurry heating in the Bayer Alumina process.

The simulations show that the standard TEMA side entry header design has very poor hydrodynamics as evaluated by the velocity angle at the tube sheet. An alternative design using axial entry with a flared inlet nozzle has considerably better hydrodynamics but the behaviour is influenced considerably by inlet pipe configuration.

REFERENCES

- BREMHORST, K, and BRENNAN, M., (2009), "CFD modelling of alumina slurry heat exchanger headers: (i) Comparison of CFD approaches", Seventh Int. Conf. on CFD in the Minerals and Process Industries, CSIRO< Melbourne, Australia, 9-11 Dec., paper 105BRE.
- BREMHORST, K. and FLINT, P.J., (1991), "The effect of flow patterns on the erosion/corrosion of shell and tube heat exchangers", *Wear*, 145, 123-135.
- FLUENT 6.3 Users Guide (2006), Fluent Inc, Lebanon NH.
- MULLEY R. (2004), "Flow of industrial fluids - Theory and equations", Ch 1-4, 11, CRC Press, Boca Raton, Florida, USA
- LAI, J.C.S., and BREMHORST, K., (1979), "Control of corrosion-erosion of tube inlets of shell and tube heat exchangers". *Wear*, 54, 1, 101-112, May.
- MENTER F. R. (1992), "Improved two equation $k-\omega$ turbulence models for aerodynamics flows", NASA TM-103975.
- WILCOX D. C. (1998), "Turbulence modelling for CFD", 2nd Edition DCW Industries, La Canada, California.